AECL-5999

ATOMIC ENERGY OF CANADA LIMITED

L'ÉNERGIE ATOMIQUE DU CANADA LIMITÉE

CONVERGENT BEAM THICKNESS DETERMINATION OF THIN FOIL ZIRCONIUM SPECIMENS

by

C. D. Cann

Whiteshell Nuclear Research Establishment

Pinawa, Manitoba R0E 1L0

1978 July

ATOMIC ENERGY OF CANADA LIMITED

CONVERGENT BEAM THICKNESS DETERMINATION OF THIN FOIL ZIRCONIUM SPECIMENS

by

C.D. Cann

Whiteshell Nuclear Research Establishment
Pinawa, Manitoba ROE 1LO

1978 July

AECL-5999

DETERMINATION DE L'EPAISSEUR DE FEUILLES MINCES DE ZIRCONIUM PAR FAISCEAUX CONVERGENTS

par

C.D. Cann

RESUME

L'utilisation de configurations de faisceaux convergents pour déterminer l'épaisseur d'une feuille de zirconium examinée au microscope électronique a été étudiée sur le plan théorique et expérimental. Selon les calculs dynamiques théoriques de faisceaux multiples, les réflexions $[10\bar{1}2]$ $[10\bar{1}3]$ et $[11\bar{2}0]$ à une tension d'accélération de 100 kV et les réflexions $[10\bar{1}3]$, $[11\bar{2}0]$ et $[11\bar{2}2]$ à 200 kV sont les plus appropriées pour la détermination de l'épaisseur par faisceaux convergents. Des configurations expérimentales de faisceaux convergents ont été obtenues avec le microscope électronique JEOL-200B dans deux séries de conditions basées sur la taille de la configuration désirée. L'analyse des configurations obtenues, effectuée avec l'aide d'un ordinateur, ont donné des épaisseurs de feuilles qui étaient en bon accord avec les épaisseurs obtenues par la méthode des franges d'égale épaisseur.

L'Energie Atomique du Canada, Limitée
Etablissement de Recherches Nucléaires de Whiteshell
Pinawa, Manitoba ROE 1LO
1978 juillet

AECL-5999

CONVERGENT BEAM THICKNESS DETERMINATION OF THIN FOIL ZIRCONIUM SPECIMENS

by

C. D. Cann

ABSTRACT

The use of convergent beam patterns to determine the thickness of zirconium foils observed in the electron microscope has been investigated both theoretically and experimentally. On the basis of many-beam dynamical theory calculations, the $[10\bar{1}2]$ $[10\bar{1}3]$ and $[11\bar{2}0]$ reflections at an accelerating voltage of 100 kV and the $[10\bar{1}3]$, $[11\bar{2}0]$ and $[11\bar{2}2]$ reflections at 200 kV were found most suitable for convergent beam thickness determinations. Experimental convergent beam patterns were obtained in the JEOL-200B electron microscope under two different sets of conditions based on the size of the pattern desired. Computer assisted analysis of the patterns obtained gave foil thicknesses in good agreement with those determined from thickness extinction contours.

Atomic Energy of Canada Limited
Whiteshell Nuclear Research Establishment
Pinawa, Manitoba ROE 1LO
1978 July

AECL-5999

CONTENTS

1. INTRODUCTION

The available procedures for preparing thin foils of zirconium for observation in the electron microscope result in specimens of unknown thickness. An area suitable for examination may vary in thickness from less than 10 to greater than 500 nm. For some investigations, knowledge of the exact thickness is required, notably for certain radiation damage studies. One parameter, necessary in these studies, is the density of radiation-induced defects resulting from a given irradiation. Since the electron microscope condenses the three-dimensional array of defects into a two-dimensional image, this parameter cannot be obtained unless the thickness of the specimen at the point of observation is known.

Specimen thickness may also be a factor in the identification of the type of radiation-induced defect. For small, point defect agglomerates, it has been shown that the usual method for determining type (vacancy or interstitial) based on the direction of the black-white contrast may be in error if the thickness of the foil is not taken into consideration[1]. In addition, when characterizing defects by comparison with computer-simulated electron microscope images, good agreement will depend upon an accurate knowledge of the foil thickness for use as a parameter in the computer program[2].

A number of methods[3] are available for determining foil thickness, although not all are suitable for zirconium specimens. The first of these involves tilting the specimen so that a set of thickness extinction contours is visible. Since each successive contour, as counted in from the specimen's edge, corresponds to an increase of one extinction distance in depth, a count of these contours and a knowledge of the extinction distance[4] will give the foil thickness. This technique has the stringent condition, however, that the exact Bragg condition be fulfilled for the imaging reflection and is most accurate for uniform

wedge-shaped foils. When rounding of the foil edge occurs during specimen preparation, or relatively flat foils are examined, errors may arise in determining the number of fringes. This error may also occur in irradiated specimens where the fringes are obscured by the irradiation damage.

A second technique for measuring foil thickness utilizes the projected width of an object lying on a known plane and cutting both surfaces of the foil. Such objects may be stacking faults, precipitates or slip traces. In the case of zirconium and its alloys of interest, neither stacking faults nor, generally, precipitates of suitable morphology occur. In annealed zirconium, dislocation slip traces are often observed and, in fact, may be so numerous that they overlap and thereby complicate the thickness determination due to the difficulty of identifying the intersections of a particular trace with the top and bottom surfaces. In irradiated material, these slip traces are generally not observed because individual dislocation movement is restricted by the dislocation tangles arising from the irradiation. Thus, their presence for use in thickness determination in irradiated materials would be fortuitous.

A third technique for thickness determination involves the recording of stereo pairs of electron micrographs. In this technique, the parallax for a pair of objects on opposite surfaces of the foil is measured and related to the foil thickness through an algebraic relationship. This technique, although simple in theory, is often difficult to apply in practice. Difficulties in tilting the specimen to record good stereo images, as well as in finding suitable surface structures for measuring the parallax, can significantly affect the accuracy of the technique.

A fourth technique for determining foil thickness is based on the analysis of the fine structure observed in convergent beam patterns[5,6]. These patterns are obtained by allowing a highly convergent

beam of electrons to be incident upon the specimen in place of the nearly parallel beam of normal microscopy. If a detailed comparison between the experimental fine structure and that theoretically predicted is carried out, thickness values to within one or two atomic layers may be obtained in instruments specifically designed for convergent beam studies[7,8]. Recently, however, Kelly and co-workers[9] have studied the convergent beam patterns generated in a scanning transmission electron microscope and have shown that these also can be used to give accurate values for the foil thickness. In this instrument and using a simple technique for analysing the patterns, they obtained thicknesses to within two percent accuracy for different cubic materials. Such accuracy is significantly better than that obtained in the previously described techniques, where thicknesses are generally quoted to within only 10 percent.

Based on the encouraging results of Kelly and co-workers[9], we decided to investigate the feasibility of using convergent beam techniques for thickness determinations in the hexagonal phase of zirconium. The JEOL-200B microscope, although currently not operable as a scanning instrument, does have the capability for strongly exciting the objective lens, a feature necessary for the generation of convergent beam images. Using this instrument, the operating conditions for obtaining convergent beam patterns were first determined. Then, zirconium samples were examined and the specimen conditions necessary to obtain convergent beam patterns suitable for thickness determination were investigated.

2. ORIGIN AND ANALYSIS OF CONVERGENT BEAM PATTERNS

In the transmission electron microscope, a beam of high energy electrons is focussed on a thin foil specimen. If this specimen is crystalline, the electrons, while passing through it, interact strongly with the periodic electric field of the crystal. This interaction

results in Bragg scattering of some of the electrons to form diffracted beams. In addition, the intensity of each of these beams is modulated to vary periodically with depth in the specimen. The period of this modulation, termed the extinction distance, depends upon the lattice potential and is, thus, different for each type of diffracted beam.

In the two-beam approximation of the dynamical theory of electron diffraction[10], only the directly transmitted and the most strongly diffracted beams are considered. In this case, the extinction distances, ξ, of the diffracted beam can be written

$$\xi = \xi_g / \sqrt{1 + \xi_g^2 s^2} \qquad (1)$$

Here ξ_g is the extinction distance at the exact Bragg[7] condition for the diffracted beam, g, and s is a parameter giving the deviation of the diffracted beam from this condition for the specimen orientation of interest. Since ξ is a function of s, the diffracted beam intensity at the bottom of a specimen of constant thickness will vary as s is changed. A plot of this variation is called a rocking curve and an example of one such curve is shown in Figure 1(a). Here the intensity of the (220) reflection in silicon is plotted as a function of s for a specimen thickness of 170 nm and an electron accelerating voltage of 200 kV.

Experimentally, this predicted variation in beam intensity with the deviation parameter, s, may be readily observed. It is most commonly seen in the form of bend contours which are strong contrast fringes resulting from bends in the specimen. The variation is also evident in the marked changes in the intensity transmitted through different crystal grains as a specimen is mechanically tilted with respect to the incident electron beam.

In both of these cases, the variation in s causing the intensity variations lies in the local orientation of the specimen with

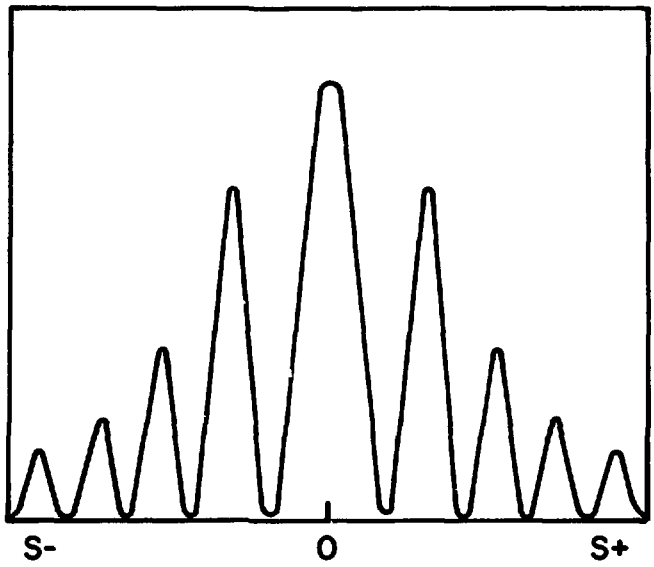

FIGURE 1 (a): Theoretical variation of the (220) diffracted beam intensity in silicon with deviation from the Bragg condition for a specimen thickness of 170 nm at an accelerating voltage of 200 kV.

FIGURE 1 (b): An experimental convergent beam disc for the (220) reflection in silicon at an accelerating voltage of 200 kV. The specimen thickness was approximately 170 nm and the variation in s across the image the same as Figure 1 (a).

respect to the incident beam. The electrons in this beam are, under standard microscope conditions, nearly parallel in their movement, with typical beam divergences of approximately 10^{-4} rad. If, however, the electron beam incident on the specimen is strongly converging, a convergent beam pattern may be obtained. This pattern has the appearance of a normal electron diffraction pattern except that each spot is replaced by a much larger disc whose diameter depends upon the convergence of the incident beam. If a number of diffracted beams are simultaneously strongly excited, the intensity variations in the discs corresponding to each may be complicated. If only one diffracted beam is strongly excited, however, the contrast appears as a series of parallel light and dark fringes, such as shown in Figure 1(b). The fringes in this convergent beam disc result from the variation of ξ with s, where s is changing due to the angular spread in the directions of the electrons in the incident beam. The variation in s horizontally across the disc is the same as that in Figure 1(a). As can be seen by comparing these two figures, the minima in the rocking curve appear as dark fringes in the convergent beam disc while the maxima correspond to regions of high intensity.

An inspection of Figures 1(a) and 1(b) reveals that the intensity varies periodically with s and this is indeed true for all thicknesses. For a particular thickness t, the first minimum in the plots occurs at a value of s such that $t = m\xi$ where m is an integer. The second minimum occurs at a larger value of s such that $t = (m+1)\,\xi$ etc.

For the i'th minimum we can then write

$$\frac{t}{n_i} = \xi = \frac{\xi_g}{\sqrt{1 + \xi_g^2 s_i^2}} \qquad (2)$$

where n_i is a positive integer. By squaring both sides and rearranging we then obtain

$$\left(\frac{s_i}{n_i}\right)^2 + \left(\frac{1}{n_i^2}\right)\left(\frac{1}{\xi_g^2}\right) = \frac{1}{t^2} \qquad (3)$$

This last equation is the expression used by Kelly and co-workers [9] in their convergent beam thickness determinations. They measured s_i for a series of consecutive fringes in a convergent beam pattern and then plotted

$$\left(\frac{s_i}{n_i}\right)^2 \text{ versus } \frac{1}{(n_i)^2} \text{ for } n_1 = 1,2,3\ldots \text{ and } n_i = n_1 + i - 1$$

until the best straight-line plot was obtained. The intercept of this line with the $\left(\frac{s_i}{n_i}\right)^2$ axis gives $\frac{1}{t^2}$ while the slope is equal to $1/\xi_g^2$.

The strongly convergent beam required to generate the convergent beam patterns is obtained through appropriate adjusting of lens excitations in a transmission electron microscope, as shown schematically in Figure 2. A beam of electrons, issuing from a thermionic or field emission source, is focussed by the first condenser lens to form a demagnified image of the electron source, typically 1 μm in diameter. The second condenser lens is then underfocussed while the objective lens is very strongly excited so that its magnetic field above the specimen or, pre-field, acts to focus the beam into a fine probe at the specimen. This probe is typically 10 nm or less in diameter and has a beam divergence, α_c, of the order 5×10^{-2} rad, depending upon the first condenser lens excitation and the second condenser aperture, as well as the second condenser and objective lens currents. The directly transmitted and diffracted beams leaving the bottom surface of the specimen are then imaged, as shown in Figure 2, to give the convergent beam images on the

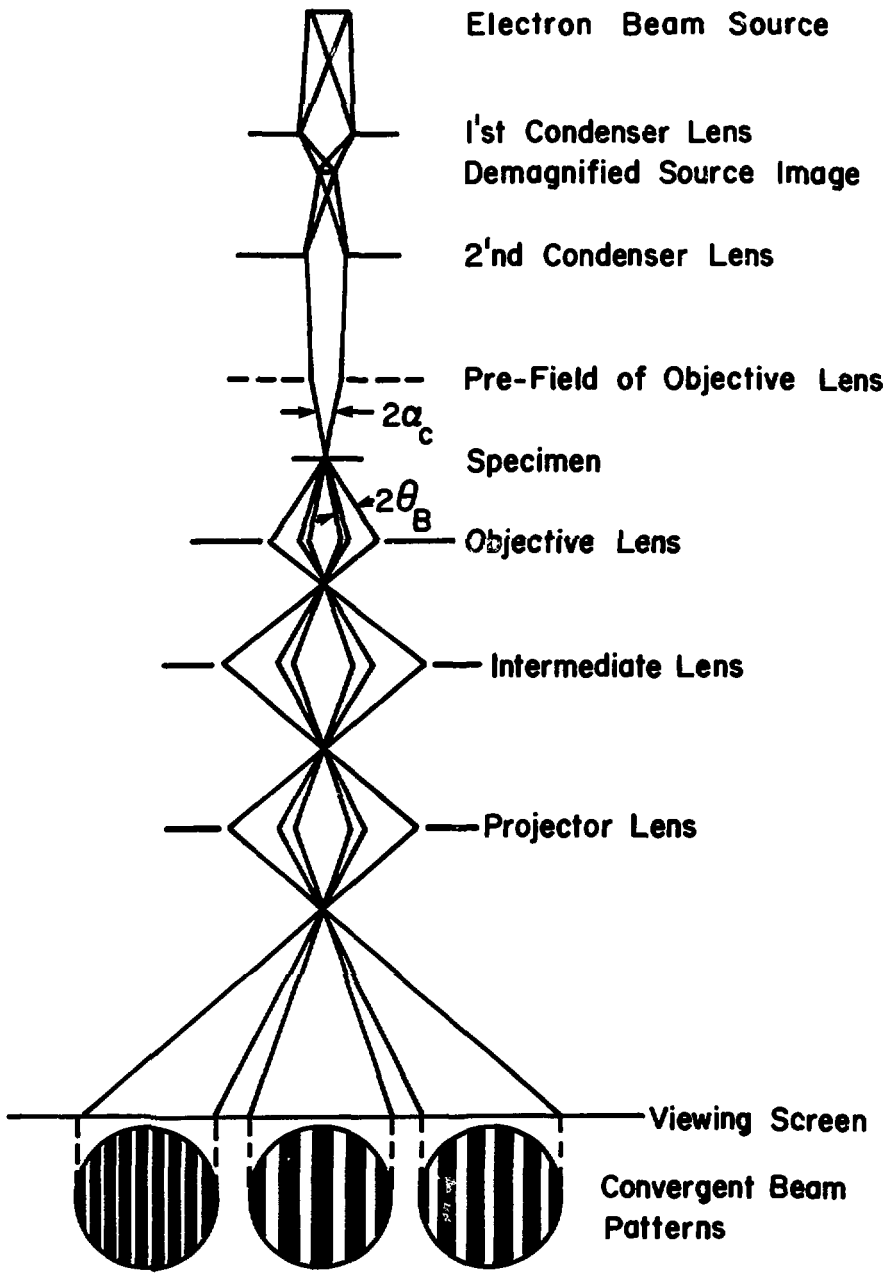

FIGURE 2: A schematic diagram showing the generation of a convergent beam pattern in a transmission electron microscope.

viewing screen. In this imaging process, the excitations of the intermediate and projector lens are adjusted to values which, under normal microscope operating conditions, would result in a low magnification ($\sim$ 2000 X) image.

3. GENERATION OF CONVERGENT BEAM PATTERNS IN THE JEOL-200B ELECTRON MICROSCOPE

Several sets of conditions were found under which convergent beam patterns could be obtained in the JEOL-200B microscope. Two of these sets of conditions will be described here. The first set is suitable for lower order reflections, i.e. where the convergent beam discs of both the directly transmitted and diffracted beams can be recorded on the same electron micrograph. This is the case assumed by Kelly and co-workers[9]. The second set is suitable for higher order reflections and for certain orientations involving lower order reflections such as where both the directly transmitted and diffracted beam discs cannot be recorded on the same micrograph. In this case, only the diffracted beam disc is recorded and a standard set of conditions employed.

These two sets of conditions for obtaining convergent beam images are shown in Table 1, along with standard diffraction settings for comparison.

The procedure for obtaining convergent beam images is basically the same for both the transmitted and diffracted beams (TDB) and diffracted beam only (DBO) modes. This procedure is as follows:

1. Under normal imaging conditions, centre the image of the area of interest of the specimen on the fluorescent viewing screen.

TABLE 1

LENS CURRENTS AND SWITCH SETTINGS UNDER STANDARD DIFFRACTION AND CONVERGENT BEAM IMAGING MODES

Setting	Standard Diffraction	Convergent Beam Transmitted and Diffracted Beams	Convergent Beam Diffracted Beam Only
1'st Condenser Lens	37.0 mA	37.5 mA	37 - 37.5 mA
2'nd Condenser Lens	51.3 mA	42.0 mA	49.5 mA
Objective Lens	50.0 mA	63.2 mA	60.0 mA
Intermediate Lens	77.5 mA	16.0 mA	67.1 mA
Projector Lens	77.2 mA	77.2 mA	43.0 mA
FUNCTION (magnification)	SA DIFF	M2	M1
FUNCTION (objective lens)	EM	SM	SM
Condenser Lens Aperture	200 μμ ϕ	60 μμ ϕ	200 μμ ϕ
Projector Lens Pole Piece	In	Out	In

2. While maintaining this area on the screen, tilt the specimen until a suitable Bragg reflection is found and good two-beam conditions obtained. The specimen should be oriented so that the reflection fulfills the Bragg condition.

3. Set the magnification at the SA IMAGE setting and focus the image using the objective lens. Record this focussing current in the DBO case.

4. Remove the objective and selected area apertures from the beam path.

5. Insert and centre the appropriate condenser lens aperture.

6. Turn the FUNCTION knob (magnification) to the appropriate M range (M2 for TDB or M1 for DBO) and adjust the magnification current to ∿ 16 mA for the TDB case, or exactly 43 mA in the DBO case.

7. Remove the projector lens pole piece in the TDB case by first shutting off the projector lens and then unscrewing and pulling out the pole piece. Turn the projector lens back on once the pole piece is removed.

8. Turn the FUNCTION switch on the objective lens control unit to SM.

9. Adjust the objective lens current to ∿ 60 mA using the controls on the lens control unit.

10. Reduce the current in the second condenser lens by approximately 9 mA (TDB) or 2 mA (DBO), using the main console controls.

11. Centre the desired area of the convergent beam pattern on the fluorescent screen using the BRIGHT FIELD X-Y controls on the objective lens control unit. The DF/OFF/BF knob must be set at BF for these controls to be operable.

12. Fine adjust the objective and second condenser lens currents until a convergent beam pattern of a suitable size is obtained. Record the objective lens current.

    Note that low magnification images of the specimen are obtained for over and underfocus values of the objective lens current. As the convergent beam condition is approached, the magnification of this image becomes larger and the image appears to go out of focus until the fringes appear. Generally, if good two-beam conditions prevail, the convergent beam pattern is in focus when the fringes are parallel and running perpendicular to a line joining the directly transmitted and diffracted spots.

In the procedure described by Kelly and co-workers[9] for obtaining convergent beam patterns, they switched directly from the scanning transmission mode to the convergent beam condition by stopping the beam at the desired position on the specimen and recording the convergent beam pattern immediately on a micrograph. This is easily accomplished since the electron beam used in scanning mode is already strongly convergent. In our case, the positioning of the beam on the specimen is complicated by the shifting of the beam when the objective

lens is more strongly excited in going from conventional transmission microscopy to the convergent beam mode. In fact, because of this shift, the actual position of the beam on the specimen is not known before the convergent beam pattern is recorded. This position can usually be found after the pattern is recorded, however, by the appearance of a heavily contaminated area on the specimen at the point of measurement. Contamination develops quite rapidly in the highly focussed beam and the resulting contamination spot is generally obvious.

This rapid build-up of contamination can be very detrimental in convergent beam work. It may occur so rapidly that the fringes in the convergent beam pattern disappear before the pattern can be recorded photographically. With the excellent cold-trapping on the JEOL-200B, the contamination rate is low enough that the patterns remain visible for the order of 15 s, long enough to allow their recording. It was noted, however, that specimens left in the microscope for extended periods without liquid nitrogen in the cold traps became contaminated significantly more rapidly than when first inserted even after the traps had been refilled. In addition, the flooding technique suggested by Rackham and Eades[11] for reducing contamination was attempted but found not to affect the contamination rate significantly.

4. ANALYSIS OF CONVERGENT BEAM PATTERNS

Kelly and co-workers[9] analysed their convergent beam patterns for specimen thickness using the previously described equation

$$\left(\frac{s_i}{n_i}\right)^2 + \left(\frac{1}{n_i^2}\right)\left(\frac{1}{\xi_g^2}\right) = \frac{1}{t^2} \qquad (3)$$

This equation was developed from the two-beam approximation of the dynamical theory of electron diffraction and is, strictly speaking,

valid only under exact two-beam conditions, i.e. when only the directly transmitted beam and one strong diffracted beam are visible in the diffraction pattern.

In actual practice, two-beam conditions are never fully realized. However, by tilting the specimen with respect to the electron beam, orientations can be obtained at which only one row of diffraction spots is strongly excited. The higher order reflections in this row, termed the systematic reflections, will always be present and may have a marked effect on the extinction distance and its variation with s[12,13]. In general, the effects of these reflections become less when first order diffracted beams with smaller planar spacings are chosen. However, this advantage must be weighed against the low intensities and large extinction distances of such reflections, two factors which can severely restrict their use for thickness determinations.

Kelly and co-workers[9], in their thickness measurements in cubic metals, suggested using reflections with planar spacings between 0.07 and 0.13 nm to optimize the conditions for the convergent beam techniques. In hexagonal materials, the situation is more complex due to the different structure factors for different reflections. To find suitable reflections in this material, we calculated theoretical convergent beam patterns, using the ten-beam approximation of the dynamical theory in which eight systematic reflections were included in addition to the directly transmitted and desired diffracted beams. These patterns were then analysed using the two-beam formula and the results compared, both with respect to thickness and extinction distance, to the actual values of these parameters used in the calculations.

As expected, the lowest order reflections [$10\bar{1}0$], [0002] etc. showed poor agreement between the thicknesses calculated from the patterns and those used in the calculation of these patterns. For some higher order reflections however, we did find good agreement both with respect to thickness and extinction distance. These reflections are listed in

Table 2 along with the range of thicknesses for which good agreement was found.

TABLE 2

REFLECTIONS SUITABLE FOR CONVERGENT BEAM THICKNESS DETERMINATION IN ZIRCONIUM AT ACCELERATING VOLTAGES OF 100 AND 200 kV

100 kV		200 kV	
Reflection	Thickness Range (nm)	Reflection	Thickness Range (nm)
$10\bar{1}2$	80.0 - 350.0	$10\bar{1}3$	40.0 - 350.0
$10\bar{1}3$	30.0 - 250.0	$11\bar{2}0$	50.0 - 200.0
$11\bar{2}0$	30.0 - 150.0	$11\bar{2}2$	40.0 - 300.0

The minimum thickness for which a reflection can be used to give a thickness determination is determined by both the extinction distance of that reflection and the beam divergence in the convergent beam patterns. For the calculations described here, the maximum physically realistic beam divergence of a Bragg angle for the reflection of interest, was used. Divergences greater than this result in overlapping of convergent beam images. The maximum thickness is determined by absorption of the material, as well as the ability to resolve the fringes in the convergent beam images. The number of fringes increases quite rapidly with increasing thickness and the resolution of these fringes is hindered in thick crystals by the contribution of inelastically scattered electrons to the overall background[8], as well as by the rapid contamination buildup on the surface.

In their two-beam analysis of convergent beam patterns to determine specimen thickness, Kelly and co-workers[9] plotted

$$\left(\frac{s_i}{n_i}\right)^2 \quad \text{versus} \quad \frac{1}{n_i^2} \quad \text{for}$$

$n_1 = 1,2,3, \ldots$ and $n_i = n_1 + i - 1$ until the best straight-line fit for the data was obtained and the slope of the line gave a value of extinction distance in reasonable agreement with the computed many-beam extinction distance. The main drawback with this approach is the time involved in generating such plots. Depending on the thickness of the specimen, as many as five plots may be required before a good fit is obtained.

In our work, a numerical technique was developed to eliminate the plotting step. A straight line was fitted to the data for each of $n_1 = 1,2,3, \ldots$ using a least-squares technique[14] and the thickness and extinction distance calculated from the line. By examining both the extinction distances and the fit of the lines to the data, the best value for n_1 was chosen and the corresponding value of the thickness, t, determined. To carry out this calculation rapidly, a Fortran computer program was written for the on-site PDP-10 computer (Appendix A).

In analysing a convergent beam pattern the deviation parameter s_i must be determined for each fringe. This parameter is defined as equal to $g\,\Delta\theta_i$ where g is the reciprocal lattice vector corresponding to the diffracted beam of interest and $\Delta\theta_i$ is the angular deviation from the exact Bragg condition, measured in radians. Substituting 1/d for g and multiplying $\Delta\theta_i$ by $\theta_B/\lambda/2d$, where θ_B is the Bragg angle for the reflection and is to a good approximation, equal to $\lambda/2d$ from Bragg's Law for the small angles involved here, the following equation is obtained

$$s_i = \frac{\lambda}{d^2} \quad \frac{\Delta\theta_i}{2\theta_B} \qquad (4)$$

In this equation, λ is the relativistic wavelength of the incident electrons, d is the interplanar spacing and the ratio $\Delta\theta_i/2\theta_B$ is equal

to the ratio of the distance of the i'th fringe from the centre of symmetry in the diffracted beam convergent beam pattern, to the spacing between the directly transmitted and diffracted convergent beam image discs.

In the TDB case here as in the situation described by Kelly and co-workers[9], the convergent beam patterns are recorded such that the images of both the directly transmitted and diffracted convergent beam discs appear on the same photographic plate. The ratio $\Delta\theta_i/2\theta_B$ for the i'th fringe can then be found directly from this plate by measuring the distance from the centre of symmetry of the diffracted convergent beam disc to the i'th dark fringe, as well as the distance between the directly transmitted and the diffracted beam discs. The ratio of these two distances is equal to $\Delta\theta_i/2\theta_B$.

In the DBO case, however, only the diffracted convergent beam disc is recorded. When doing this, a higher magnification image is obtained, facilitating the rapid focussing of the image to minimize the effects of contamination, as well as aiding the subsequent measurement of the fringe spacings. The use of these large images, however, precludes the measurement of $2\theta_B$ on the photographic plates.

To obtain values for $2\theta_B$, the magnification of the convergent beam image was calibrated as a function of objective lens excitation for fixed intermediate and projector lens currents. As the specimen lies within the magnetic field of the objective lens, small changes in specimen height also affect this magnification and this was taken into account in the calibration. This calibration was carried out by measuring the variation in the (0002) diffraction spot spacing in zirconium as a function of objective lens current for different specimen heights. This spacing was then used to evaluate a parameter K such that

$$\frac{1}{2\theta_B} = K\,d \qquad (5)$$

where d is the interplanar spacing for the set of planes corresponding to the Bragg angle θ_B and $2\theta_B$ corresponds to the distance (cm) between the discs in a convergent beam pattern.

The results of this calibration are shown in Figure 3. Here K is plotted as a function of the objective lens current for currents in the range 59 to 66 mA and for specimen heights corresponding to focussing currents under SA conditions of 48, 49, 50 and 51 mA. Variation of K with second condenser lens current was examined and, as expected, was found to be independent of this current. Similarly, varying the second condenser aperture size or first condenser lens current did not affect K, although they have a marked effect on the beam divergence.

To use Figure 3 to obtain a value for 2θ, it is first necessary to focus the image of the specimen under SA conditions and record the objective lens current. This current is directly related to the height of the specimen in the objective lens. A convergent beam image is then obtained and the new objective lens current recorded. With these two values, a value for K can be found from Figure 3 by interpolation and 2θ evaluated.

5. EXPERIMENTAL RESULTS

Thickness determinations were carried out using both the TDB and DBO techniques and good results obtained. Since the TDB technique and subsequent analysis of results have been well described by Kelly and co-workers[9] the emphasis in the results described here will be on the DBO method.

A number of zirconium specimens were examined for relatively strain-free, wedge-shaped regions. When such a region was found, the specimen was tilted until a $(10\bar{1}3)$ reflection was obtained in the exact

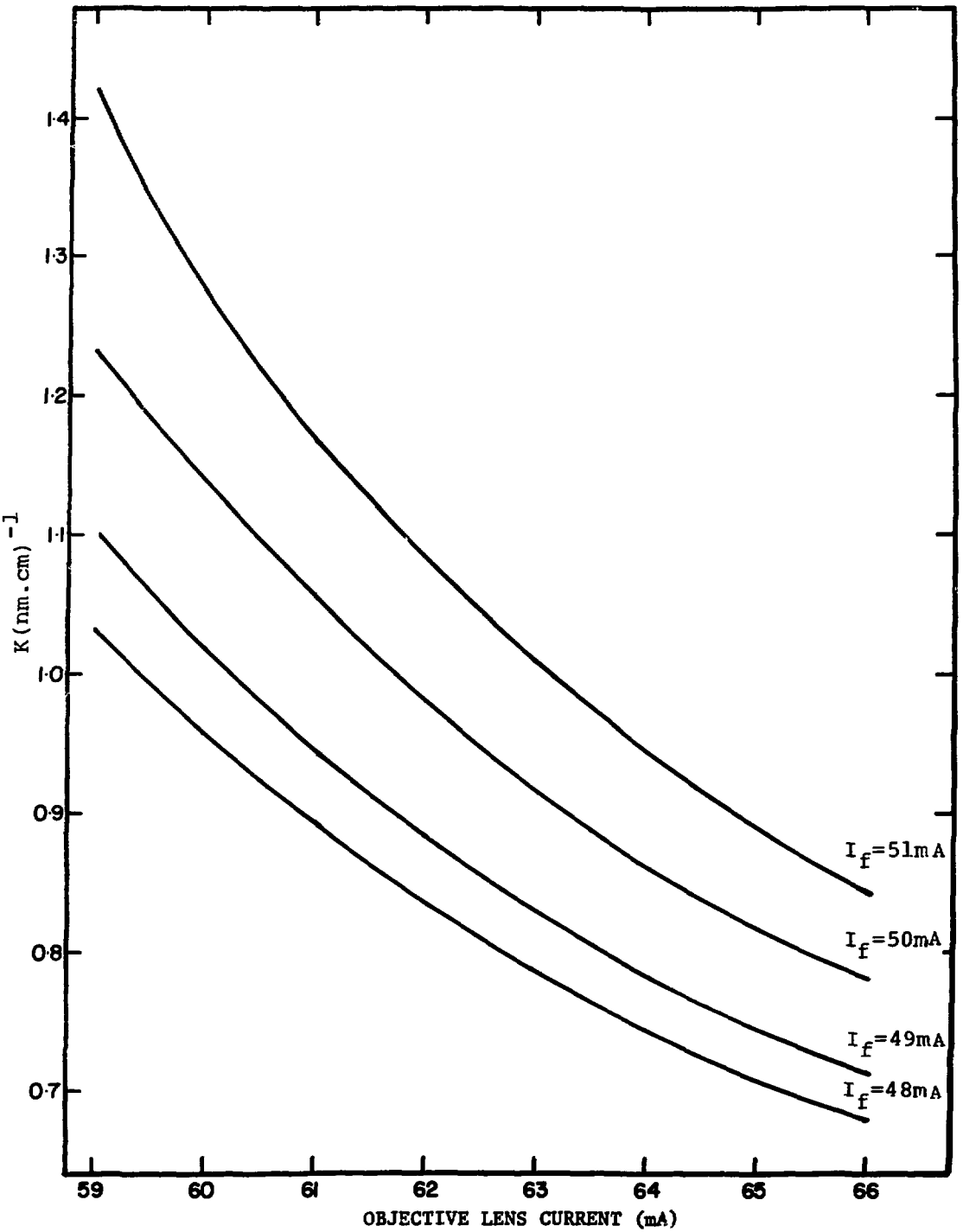

FIGURE 3: The variation of $K = 1/2\theta_B d$ with objective lens focussing current and objective lens convergent beam imaging current.

Bragg condition and no other low-order reflections, with the exception of the $(10\bar{1}3)$ systematics, were strongly excited. Convergent beam patterns were then obtained for a series of positions of increasing thickness. Following this, the specimen was imaged using standard conditions and the contamination spots corresponding to these positions recorded on a micrograph along with the thickness extinction contours. By determining the position of the contamination spots with respect to these contours, an estimate was made of the thickness at each position based on the many-beam extinction distance for the $(10\bar{1}3)$ reflection[4].

One set of convergent $(10\bar{1}3)$ beam discs obtained in this manner is shown in Figure 4. The thickness of the sample is increasing in going from a to f, as can be seen by the increasing number of fringes in the discs. The focussing current for the specimen was 49 mA, while the convergent beam patterns were recorded at a current of 64 mA. From Figure 3, K is then 0.783 $cm^{-1} \cdot mm^{-1}$ and using d = 0.146? nm for the $(10\bar{1}3)$ reflection, the value of 2θ was determined to be 8.76 cm. The distances from the centre of symmetry to the 1'st, 2'nd, 3'rd, ..., dark fringes were then measured and the specimen thickness at which each pattern was recorded was found using the least-squares method described in Appendix A. The results are shown in Table 3.

The extinction contour thicknesses in Table 3 were found from the estimated positions of the corresponding contamination spots with respect to the thickness extinction contours. A bright-field micrograph of these spots is shown in Figure 5. Before recording this micrograph, the specimen was tilted slightly about the Bragg condition of the $(10\bar{1}3)$ reflection to insure that the spacing of these contours was a maximum, as occurs at the exact Bragg condition.

As can be seen in Table 3, there is good agreement between the thicknesses determined by the convergent beam method and those derived from thickness contours. This agreement is generally well within the estimated error of 0.1 ξ_o or 9 nm in the thicknesses determined using

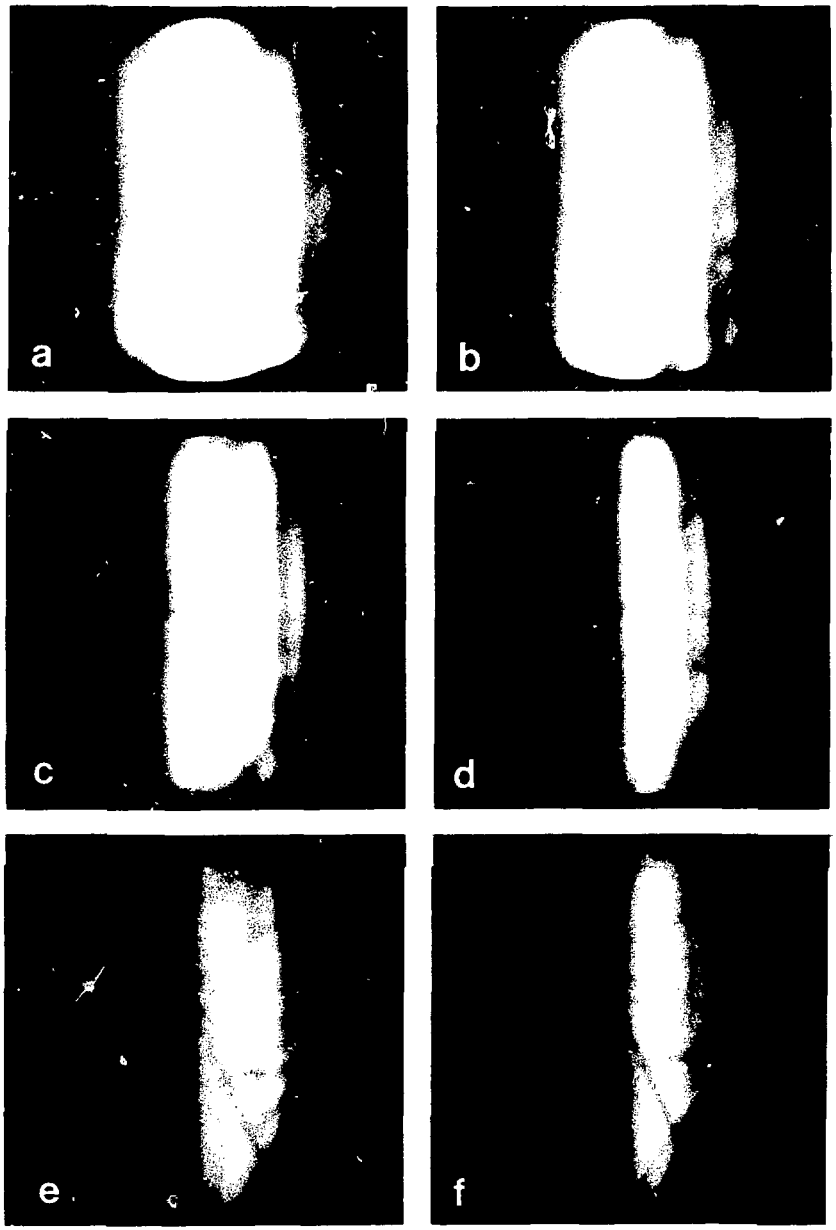

FIGURE 4: $(10\bar{1}3)$ convergent beam images in zirconium at 200 kV. The thickness of the specimen is increasing in going from a to f.

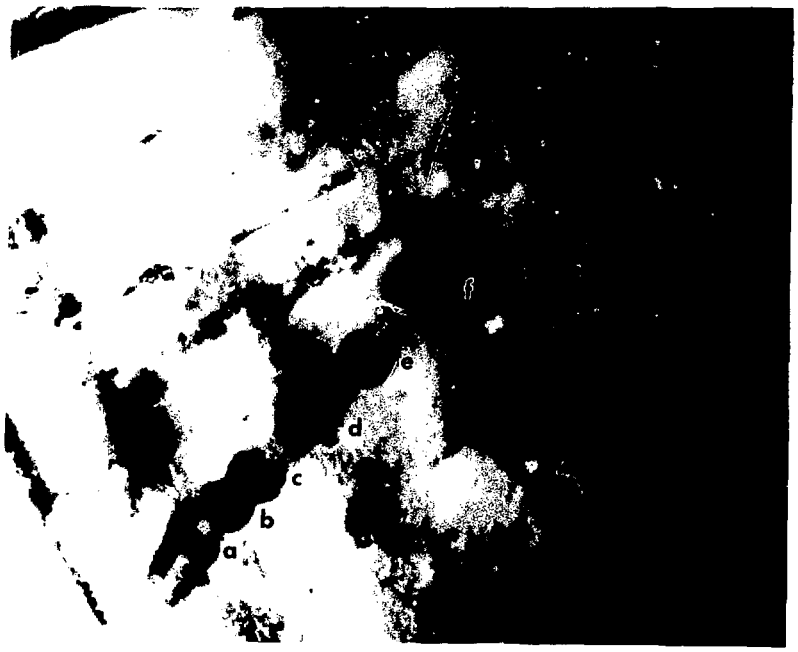

FIGURE 5: A bright-field electron micrograph of the region from which the convergent beam images in Figure 4 were recorded. The edge of the specimen is at the lower right hand corner and the contamination spots corresponding to each convergent beam image are labelled correspondingly.

TABLE 3

SPECIMEN THICKNESS DETERMINATIONS IN ZIRCONIUM USING THE $(10\bar{1}3)$ REFLECTION AT 200 kV

Specimen Position	Convergent Beam Thickness (nm)	Extinction Contour Thickness (nm)	Theoretical Extinction Distance ξ_g (nm)	Convergent Beam Extinction Distance (nm)
a	123.5	$1.45\ \xi_g = 126.7$	87.3	89.1
b	147.5	$1.75\ \xi_g = 152.8$	87.3	89.4
c	183.0	$2.0\ \xi_g = 174.7$	87.3	86.0
d	232.0	$2.5\ \xi_g = 218.0$	87.3	83.1
e	265.9	$3.0\ \xi_g = 262.0$	87.3	89.1
f	308.5	$3.5\ \xi_g = 306.0$	87.3	90.1

the extinction contour method. Subsequent measurements under similar conditions, in general, confirmed this agreement.

In Table 3, the experimental extinction distances, as determined from the slope of the least-squares fitted line are also presented for comparison with the theoretically predicted value. Here again, there is good agreement with the theoretical extinction distance. The extinction distances, determined during the subsequent thickness measurements mentioned in the previous paragraph, did not exhibit such good agreement, but generally were within 15 percent of the theoretical value.

6. DISCUSSION

In their work, Kelly and co-workers[9] stated that, in every case they analysed using different materials and different reflections, the accuracy in the foil thickness determination appeared to be better

than two percent. As they had no other technique for more precisely determining the thickness, absolute values could not be given for the accuracy. Similarly, in our work with zirconium, the thicknesses determined using the convergent beam technique could only be compared with, in principle, less accurate values obtained from extinction contour measurements. Although good agreement was found between these two sets of results, it is useful to examine possible sources of error in the technique. The two most probable sources are the value of the accelerating voltage of the microscope and the evaluation of the ratio $\Delta\theta_i/2\theta_B$.

The maximum nominal accelerating voltage of the JEOL-200B electron microscope is 200 kV. The actual value of this voltage, however, can be found only from high resolution diffraction experiments. Moreover, this voltage may change over a period of time due to changes, in the reference batteries and resistors. Calculations showed that a five percent change in the accelerating voltage would result in a corresponding six percent change in the measured thickness because of the change in the relativistic wavelength of the incident electrons.

In evaluating the ratio $\Delta\theta_i/2\theta_B$ from the ratio of the fringe spacing to the disc spacing, errors can arise in determining both of these spacings. In general, errors in measurement of the distance from the centre of symmetry of the fringes in the disc to each dark fringe should be random in nature, although the presence of non-systematic reflections, as evidenced by fringes running obliquely across the primary fringes, may introduce significant errors[9,15]. In determining the distance between the directly transmitted and diffracted beam discs by direct measurement, errors arise in determining corresponding points on the discs for measurement. The edges of the discs are often poorly defined, particularly for the diffracted beam disc where the low intensity at the edges is nearly equal to that of the general background. If, instead, this distance is found using the calibration curves (Figure 3), errors may occur due to either changes in the microscope operating

conditions over a period of time or to reading of the lens currents required for determining K from the calibration curves. The effect of a five percent error in this disc spacing was found to give a corresponding five percent error in the thickness.

Through careful reading of the lens current meter and monitoring of the diffraction spot current to detect high voltage variations, the errors in the high voltage and 2θ should both be well within five percent. The total systematic error should then be much less than the maximum 10 percent error calculated to occur when these parameters were simultaneously in error by 5 percent. If significantly higher accuracies are desired, actual measurements of the accelerating voltage and careful determination of the disc spacing for the exact conditions used would be required.

The large variations in the extinction distance, ξ_g, that were observed in the course of the thickness determinations can be, at least partially explained by the technique used to determine this parameter. It is found by evaluating the square root of the inverse of the slope of the least-squares fitted line. This slope is quite small and, thus, is very sensitive to small rotations of the line which may result from small errors in measuring the distance to the fringes.

In general, the measured extinction distances were larger than the theoretically predicted value. Kelly and co-workers[9] also observed a similar, although generally larger, increase. They suggested that this may be due to localized beam heating of the specimen. Such heating decreases the lattice potentials through a Debye-Waller factor and, therefore, results in a larger extinction distance. The theoretical extinction distance used here was calculated assuming room temperature. A second source of error which may also contribute to this difference is the lattice potentials used in calculating ξ_g. These potentials have not been confirmed experimentally in the case of zirconium and errors in these would certainly affect ξ_g, the extinction distance.

The possibility of error in the calculated extinction distance was examined by using convergent beam techniques to measure extinction distances in silicon. The (220) reflection was chosen as previous work had shown that the effects of systematic reflections were minimal and the extinction distance was in agreement with the theoretical value[16]. The results of 21 such measurements gave an average value of 100.1 nm for this extinction distance, compared to the theoretical value of 94.6 nm. This difference of 5.5 nm compares well with the 7.6 nm difference found between the mean experimental extinction distance of 94.9 nm based on 22 measurements and a theoretical value of 87.3 nm for the $(10\bar{1}3)$ reflection in zirconium. Since the disagreement between experimental and theoretical extinction distances is of the same order in both cases, 87.3 nm does appear to be a reasonable value for the $(10\bar{1}3)$ extinction distance in zirconium at 200 kV.

An additional source of error and possible limitation on the use of the convergent beam technique for thickness determination is the presence of crystalline defects such as dislocations. These defects, through the strains they cause in the crystal lattice, can markedly affect the diffraction of electrons and, therefore, locally destroy two-beam conditions. This results in distorted convergent beam images[7] that are unsuitable for thickness measurements. This fact may limit the use of this technique in heavily irradiated materials where almost no defect free regions are observed. However, in less heavily irradiated specimens, or partially annealed samples, suitable regions should be obtainable.

7. SUMMARY

Convergent beam techniques have been applied to zirconium specimens and found suitable for thickness determination when appropriate reflections are used. Convergent beam patterns were generated in

the JEOL-200B electron microscope and used for thickness determinations although the specific area of measurement could be determined only after the measurement by location of the contamination spot. Based on the analysis of possible sources of error, the actual error in thickness determinations using this technique should be much less than 10 percent under normal conditions and can be further improved by accurate measurement of microscope parameters. Finally, a computer program has been developed to speed the analysis of the convergent beam patterns for determining specimen thickness.

8. ACKNOWLEDGEMENTS

I would like to thank Prof. S.S. Sheinin and Dr. R.A. Egerton for the use of the JEOL-100B electron microscope at the University of Alberta during the initial stages of this work and J.C. Brunel of the Physics Department at the University of Alberta for very useful discussions. The preparation of suitable samples by E.E. Sexton and R.S. Styles is also gratefully acknowledged.

9. REFERENCES

1. B. Hertel, K.H. Katerbau, and R. Bair, phys. stat. sol. (a) 41, K1 (1977).

2. A.K. Head, P. Humble, L.M. Clarebrough, A.J. Morton and C.T. Forwood, "Computed Electron Micrographs and Defect Identification", p. 79, American Elsevier, New York, (1973).

3. P.B. Hirsch, A. Howie, R.B. Nicholson, D.W. Pashley and M.J. Whelan, "Electron Microscopy of Thin Crystals", p. 415, Butterworths, London, (1965).

4. C.D. Cann, Atomic Energy of Canada Limited Report, AECL-5690 (1977).

5. W. Kossel and G. Mollenstedt, Ann. Phys. 5, 113 (1939).

6. I. Ackermann, Ann. Phys. 6, 19 (1948).

7. D.J.H. Cockayne, P. Goodman, J.C. Mills and A.F. Moodie, Rev. Sci. Instrum. 38, 1097 (1967).

8. P. Goodman and G. Lehmpfuhl, Acta Cryst. 22, 14 (1967).

9. P.M. Kelly, A. Jostsons, R.G. Blake and J.G. Napier, phys. stat. sol. (a) 31, 771 (1975).

10. A. Howie, "Techniques for Electron Microscopy", p. 449, ed. by D. Kay, Blackwell, Oxford, (1965).

11. G.M. Rackham and J.A. Eades, Optik 47, 227 (1977).

12. A. Howie and M.J. Whelan, Proc. Eur. Reg. Conf. on Electron Microscopy, Delft, Netherlands, 1, 181 (1960).

13. S.S. Sheinin, phys. stat. sol. 21, 247 (1967).

14. R.G. Stanton, "Numerical Methods for Science and Engineering", p. 52, Prentice Hall, Englewood Cliffs, USA, 1961.

15. J.M. Corbett, p. 100, 4'th Ann. Proc. Microscopical Society of Canada, London, Ont., 1977, J.M. Sturgess (ed).

16. C.D. Cann, M.Sc. Thesis, University of Alberta, Edmonton, (1967).

APPENDIX A

COMPUTER PROGRAM TO ANALYSE CONVERGENT BEAM PATTERNS

In their analysis of the convergent beam fringe patterns to determine specimen thickness, Kelly and co-workers[9] plotted $(s_i/n_i)^2$ versus $(1/n_i)^2$ for $n_1 = 1,2,3,\ldots$ and $n_i = n_1 + i - 1$ until the best linear configuration of the points was obtained. The intercept of the line drawn through these points with the $(1/n_i)^2 = 0$ axis was then used to calculate the thickness. As a further check, when a number of lines appeared possible, the slope of each line was found and the extinction distance then calculated for each line and compared with the theoretical value.

This approach is straightforward but also time consuming in that a new plot must be made for each n_1 value due to the large change in scale between $n_1 = m$ and $n_1 = m + 1$. To overcome this drawback, a computer program was written to find, using a least-squares method[14], the best straight line through the points as n_i varied from 1 to 10. For each line the program calculates the extinction distance, the specimen thickness and the fit of the line to the data. These parameters are written out for those lines whose slopes give extinction distances between 0.5 and 1.5 of the theoretical value.

In our work, it was usually found that the line with the extinction distance equal to, or slightly greater than, the theoretical value had the best fit with the data. Moreover, in comparing the thickness of the specimen as determined from extinction contour measurements with the thickness predicted by the various lines, the line with this extinction distance was found to give best agreement.

Choosing the line with a corresponding extinction distance equal to, or greater than, the reference value is consistent with localized heating of the specimen in the beam. This heating would tend to decrease lattice potentials through a Debye-Waller correction and thereby result in a larger extinction distance. Also, this choice is consistent with the the results of Kelly and co-workers[9].

Although the values listed under "GOODNESS OF FIT" in the output, generally show a minimum for this line, this is not always the case. Moreover, smaller values are invariably obtained as n_i approaches 10. This latter behaviour results from the much smaller range of $(1/n_i)^2$ and $(s_i/n_i)^2$ as n_i becomes larger. The location of the local minimum at or near the chosen line may be influenced by this dependence on n_i, as well as small errors in measurements of the fringe spacings.

A listing of the computer program is given below, followed by an example of the input data and output for the convergent beam patterns shown in Figure 4. The output also contains values for the thickness and extinction distance, as determined from lines connecting points n_i and n_{i-1}. By observing the behaviour of these values for different i's, obviously inconsistent fringe spacings can be identified and checked.

```
C
C     PROGRAM CBTHIX
C
C        PURPOSE-TO CALCULATE SPECIMEN THICKNESS FROM FRINGE SPACINGS IN
C                CONVERGENT BEAM PATTERNS IN ZIRCONIUM
C
C        METHOD -A LEAST SQUARES METHOD IS USED TO GENERATE A SET OF
C                STRAIGHT LINES THROUGH THE DATA FOR N/SUB/1 EQUAL TO 1,
C                2,3,...,10. THE SLOPES OF THESE LINES ARE USED TO FIND
C                A VALUE FOR THE EXTINCTION DISTANCE. THE INTERCEPT OF
C                THE LINE EQUALS 1/(THICKNESS)**2. ONLY THOSE THICKNESSE
C                CORRESPONDING TO EXTINCTION DISTANCES BETWEEN .9 AND
C                1.5 OF A REFERENCE VALUE ARE PRINTED OUT. IF NO VALUES
C                ARE FOUND BETWEEN .9 AND 1.0 OF THIS REFERENCE VALUE
C                THE THICKNESS VALUE CORRESPONDING TO THE FIRST
C                EXTINCTION DISTANCE SMALLER THAN THE REFERENCE VALUE
C                IS OUTPUT
C
C        INPUT  -CARD 1 ACCELERATING VOLTAGE AND REFLECTION FOR
C                       PATTERNS TO BE ANALYSED    FORMAT(F,4I)
C                CARD 2 FIVE CHARACTER IDENTIFICATION,TWO THETA (CM),
C                       NUMBER OF FRINGE SPACINGS, FRINGE SPACINGS (CM)
C                                                  FORMAT(A5,1X,F,I,10F)
C                       THERE IS ONE CARD 2 FOR EACH CONVERGENT BEAM
C                       PATTERN CONSIDERED
C
      DIMENSION D(10),S2(10),SL(10),S(10),SDN2(10),T(10),EX(10),E100(22)
     2,E200(22),INDX(22)
      INTEGER HH
      DATA E100/27.2,2776.5,75.3,37.5,93.8,69.0,164.7,73.3,76.7,321.4,
     2105.3,186.9,129.3,51.4,64.4,102.3,191.2,113.1,216.2,142.9,294.7,
     2229.5/
      DATA E200/33.9,1138.9,100.4,47.6,120.0,87.3,209.2,88.8,97.1,295.6,
     1133.5,271.8,163.9,64.8,81.4,129.6,242.5,143.4,274.4,181.1,373.8,
     2319.9/
      DATA INDX/22,44,20,31,42,53,64,40,51,62,73,60,82,40,62,84,50,61,72
     2,83,94,80/
C
C     READING IN THE ACCELERATING VOLTAGE AND REFLECTION USED
C
      READ(5,100)EKV,HH,KK,II,LL
C
C     CALCULATING RELATIVISTIC WAVELENGTH AND PLANAR SPACING
C
      WAVL=.1226/(SQRT(EKV*10*(1.+(0.9788E-3*EKV))))
      DPLN=1./SQRT(2./(3.*.32335**2)*(HH**2+KK**2+II**2)+(LL/.51463)**2)
C
C     CHOOSING REFERENCE EXTINCTION DISTANCE
C
      NUM=10*(IABS(HH)+IABS(KK)+IABS(II)+IABS(LL))+IABS(LL)
```

```
      DO 5 I=1,22
      IF(NUM.NE.INDX(I)) GO TO 5
      MM=I
      IF(NUM.EQ.40.AND.HH.NE.0.AND.KK.NE.0.AND.II.NE.0) MM=I+6
      IF(NUM.EQ.62.AND.HH.NE.0.AND.KK.NE.0.AND.II.NE.0) MM=I+5
      EXTO=E100(MM)
      IF(EKV.GT.150.) EXTO=E200(MM)
      GO TO 8
    5 CONTINUE
    8 CONTINUE
      DO 1 I=1,100
      E8P=999999.0
C
C     READING IN PARAMETERS FOR A CONVERGENT BEAM PATTERN
C
      READ(5,101,END=9) ID,THEX2,N,(D(J),J=1,N)
      WRITE(6,103) ID,DPLN,THEX2,WAVL,EXTO
      DO 2 J=1,N
      S(J)=WAVL/DPLN**2*D(J)/THEX2
    2 S2(J)=S(J)**2
      DO 3 K=1,10
      DO 4 J=1,N
      SDN2(J)=S2(J)/(J+K-1)**2
      IF(J.EQ.1) GO TO 4
      SL(J)=(SDN2(J)-SDN2(J-1))/(1./(J+K-1)**2-1./(J+K-2)**2)
      IF(ABS(SL(J)).LT.1.0E-15) SL(J)=-1.0E-15
      T(J)=SQRT(ABS(1./(SL(J)*(-1./(J+K-1)**2)+SDN2(J))))
      EX(J)=SQRT(ABS(1./(-SL(J))))*-SIGN(1.0,SL(J))
    4 CONTINUE
C
C     CARRYING OUT A LEAST SQUARES FIT
C
      SY2=0.0
      SXY=0.0
      SX2=0.0
      SX=0.0
      SY=0.0
      DO 7 J=1,N
      SY=SDN2(J)+SY
      X=1.0/(J+K-1)**2
      SX=SX+X
      SY2=SY2+SDN2(J)**2
      SX2=SX2+X**2
    7 SXY=SDN2(J)*X+SXY
      B=(SX*SY-SXY*N)/(SX**2-N*SX2)
      A=(SXY-SX2*B)/SX
      TA=SQRT(1./ABS(A))
      EB=SQRT(1./ABS(B))*-SIGN(1.0,B)
      FIT=SY2-A*SY-B*SXY
      IF(EB.GT.(EXTO*1.5).OR.EB.LT.(EXTO*0.5)) GO TO 3
```

```
      IF(EBP.LT.EXTO.AND.EB.LT.(.9*EXTO)) GO TO 3
      WRITE(6,104)K
      DO 10 J=1,N
      IF(J.GT.1) GO TO 6
      WRITE(6,102) D(1)
      GO TO 10
    6 WRITE(6,102) D(J),T(J),EX(J)
   10 CONTINUE
      WRITE(6,106) TA,EB,FIT
      EBP=EB
    3 CONTINUE
      WRITE(6,107)
    1 CONTINUE
    9 CONTINUE
  100 FORMAT(F,4I)
  101 FORMAT(A5,1X,F,I,10F)
  102 FORMAT(31X,F10.2,3H CM,F10.2,3H NM,6X,F10.2,3H NM)
  103 FORMAT(1H-,25X,A5,6H PLATE/32X,15HPLANAR SPACING=,F5.4,12H  TWO TH
     2ETA=,F5.2/32X,11HWAVELENGTH=,F6.5,32H  REFERENCE EXTINCTION DISTAN
     3CE=,F10.2)
  104 FORMAT(1H0,29X,8HN/SUB/1=,I2/32X,48HFRINGE SPACING   THICKNESS   E
  106 FORMAT(32X,13HLEAST SQUARES/34X,49HTHICKNESS   EXTINCTION DISTANCE
     2   GOODNESS OF FIT/34X,F7.2,3H NM,5X,F10.2,3H NM,8X,E10.4)
  107 FORMAT(1H-)
      END
```

```
INPUT DATA
    200.0,1,0,-1,3
    CJ20A,8.76,3,.87,1.60,2.25
    CJ20B,8.76,4,.57,1.27,1.83,2.36
    CJ20C,8.76,4,.87,1.40,1.83,2.30
    CJ20D,8.76,4,.53,1.00,1.40,1.73
    CJ20E,8.76,4,.75,1.11,1.47,1.77,2.06
    CJ20F,8.76,4,.50,.87,1.20,1.47,1.73

PROGRAM OUTPUT


     CJ20A PLATE
           PLANAR SPACING=.1463  TWO THETA= 8.76
           WAVELENGTH=.00251  REFERENCE EXTINCTION DISTANCE= 87.30

         N/SUB/1= 2
           FRINGE SPACING    THICKNESS    EXTINCTION DISTANCE
                0.87 CM
                1.60 CM        124.50 NM          90.30 NM
                2.25 CM        125.05 NM          92.21 NM
           LEAST SQUARES
             THICKNESS    EXTINCTION DISTANCE    GOODNESS OF FIT
              124.72 NM           90.67 NM          .2010E-13

         N/SUB/1= 3
           FRINGE SPACING    THICKNESS    EXTINCTION DISTANCE
                0.87 CM
                1.60 CM        147.32 NM          59.84 NM
                2.25 CM        141.79 NM          54.40 NM
           LEAST SQUARES
             THICKNESS    EXTINCTION DISTANCE    GOODNESS OF FIT
              144.90 NM           58.23 NM          .5180E-12


     CJ20B PLATE
           PLANAR SPACING=.1463  TWO THETA= 8.76
           WAVELENGTH=.00251  REFERENCE EXTINCTION DISTANCE= 87.30

         N/SUB/1= 2
           FRINGE SPACING    THICKNESS    EXTINCTION DISTANCE
                0.57 CM
                1.27 CM        147.31 NM          89.01 NM
                1.83 CM        150.14 NM          95.02 NM
                2.36 CM        150.52 NM          96.60 NM
           LEAST SQUARES
             THICKNESS    EXTINCTION DISTANCE    GOODNESS OF FIT
              149.02 NM           90.78 NM          .3923E-12

         N/SUB/1= 3
           FRINGE SPACING    THICKNESS    EXTINCTION DISTANCE
                0.57 CM
                1.27 CM        174.30 NM          64.80 NM
                1.83 CM        170.24 NM          61.60 NM
                2.36 CM        166.40 NM          57.38 NM
           LEAST SQUARES
             THICKNESS    EXTINCTION DISTANCE    GOODNESS OF FIT
              170.89 NM           62.99 NM          .4850E-12
```

CJ20E PLATE
PLANAR SPACING=.1463 TWO THETA= 8.76
WAVELENGTH=.00251 REFERENCE EXTINCTION DISTANCE= 87.30

N/SUB/1= 4

FRINGE SPACING	THICKNESS	EXTINCTION DISTANCE
0.75 CM		
1.11 CM	274.11 NM	94.36 NM
1.47 CM	257.30 NM	79.76 NM
1.77 CM	273.43 NM	102.62 NM

LEAST SQUARES

THICKNESS	EXTINCTION DISTANCE	GOODNESS OF FIT
267.06 NM	89.52 NM	.8483E-13

N/SUB/1= 5

FRINGE SPACING	THICKNESS	EXTINCTION DISTANCE
0.75 CM		
1.11 CM	303.04 NM	76.34 NM
1.47 CM	279.72 NM	64.59 NM
1.77 CM	293.71 NM	74.24 NM

LEAST SQUARES

THICKNESS	EXTINCTION DISTANCE	GOODNESS OF FIT
291.10 NM	71.32 NM	.6583E-13

CJ20F PLATE
PLANAR SPACING=.1463 TWO THETA= 8.76
WAVELENGTH=.00251 REFERENCE EXTINCTION DISTANCE= 87.30

N/SUB/1= 3

FRINGE SPACING	THICKNESS	EXTINCTION DISTANCE
0.50 CM		
0.87 CM	277.84 NM	117.96 NM
1.20 CM	271.39 NM	110.54 NM
1.47 CM	292.06 NM	167.85 NM

LEAST SQUARES

THICKNESS	EXTINCTION DISTANCE	GOODNESS OF FIT
278.25 NM	118.49 NM	.9713E-13

N/SUB/1= 4

FRINGE SPACING	THICKNESS	EXTINCTION DISTANCE
0.50 CM		
0.87 CM	315.04 NM	92.65 NM
1.20 CM	300.03 NM	83.82 NM
1.47 CM	317.50 NM	100.24 NM

LEAST SQUARES

THICKNESS	EXTINCTION DISTANCE	GOODNESS OF FIT
309.50 NM	90.24 NM	.3151E-13

N/SUB/1= 5

FRINGE SPACING	THICKNESS	EXTINCTION DISTANCE
0.50 CM		
0.87 CM	348.29 NM	78.72 NM
1.20 CM	326.17 NM	70.19 NM
1.47 CM	341.05 NM	78.17 NM

LEAST SQUARES

THICKNESS	EXTINCTION DISTANCE	GOODNESS OF FIT
337.44 NM	75.36 NM	.2413E-13

CJ20C PLATE
PLANAR SPACING=.1463 TWO THETA= 8.76
WAVELENGTH=.00251 REFERENCE EXTINCTION DISTANCE= 87.30

N/SUB/1= 3

FRINGE SPACING	THICKNESS	EXTINCTION DISTANCE
0.87 CM		
1.40 CM	180.35 NM	84.12 NM
1.83 CM	190.33 NM	104.78 NM
2.30 CM	177.99 NM	72.53 NM

LEAST SQUARES

THICKNESS	EXTINCTION DISTANCE	GOODNESS OF FIT
183.41 NM	87.25 NM	.4680E-12

CJ20D PLATE
PLANAR SPACING=.1463 TWO THETA= 8.76
WAVELENGTH=.00251 REFERENCE EXTINCTION DISTANCE= 87.30

N/SUB/1= 3

FRINGE SPACING	THICKNESS	EXTINCTION DISTANCE
0.53 CM		
1.00 CM	233.27 NM	93.19 NM
1.40 CM	228.93 NM	88.94 NM
1.73 CM	243.99 NM	120.11 NM

LEAST SQUARES

THICKNESS	EXTINCTION DISTANCE	GOODNESS OF FIT
233.81 NM	93.68 NM	.1518E-12

N/SUB/1= 4

FRINGE SPACING	THICKNESS	EXTINCTION DISTANCE
0.53 CM		
1.00 CM	264.51 NM	74.86 NM
1.40 CM	253.09 NM	68.78 NM
1.73 CM	265.25 NM	78.80 NM

LEAST SQUARES

THICKNESS	EXTINCTION DISTANCE	GOODNESS OF FIT
260.06 NM	73.12 NM	.4817E-13

The International Standard Serial Number

ISSN 0067-0367

has been assigned to this series of reports.

To identify individual documents in the series we have assigned an AECL-number.

Please refer to the AECL-number when requesting additional copies of this document from

Scientific Document Distribution Office
Atomic Energy of Canada Limited
Chalk River, Ontario, Canada
K0J 1J0

PRICE - $3.00 per copy